Cellular/Molecular

PP2A and GSK-3β Act Antagonistically to Regulate Active Zone Development

Natasha M. Viquez,[1] Petra Füger,[3] Vera Valakh,[1] Richard W. Daniels,[1] Tobias M. Rasse,[3] and Aaron DiAntonio[1,2]

[1]Department of Developmental Biology and [2]Hope Center for Neurological Disorders, Washington University School of Medicine, St. Louis, Missouri 63110, and [3]Junior Research Group Synaptic Plasticity and Department of Cellular Neurology, Hertie Institute for Clinical Brain Research, University of Tübingen, Tübingen D-72076, Germany

The synapse is composed of an active zone apposed to a postsynaptic cluster of neurotransmitter receptors. Each *Drosophila* neuromuscular junction comprises hundreds of such individual release sites apposed to clusters of glutamate receptors. Here, we show that protein phosphatase 2A (PP2A) is required for the development of structurally normal active zones opposite glutamate receptors. When PP2A is inhibited presynaptically, many glutamate receptor clusters are unapposed to Bruchpilot (Brp), an active zone protein required for normal transmitter release. These unapposed receptors are not due to presynaptic retraction of synaptic boutons, since other presynaptic components are still apposed to the entire postsynaptic specialization. Instead, these data suggest that Brp localization is regulated at the level of individual release sites. Live imaging of glutamate receptors demonstrates that this disruption to active zone development is accompanied by abnormal postsynaptic development, with decreased formation of glutamate receptor clusters. Remarkably, inhibition of the serine-threonine kinase GSK-3β completely suppresses the active zone defect, as well as other synaptic morphology phenotypes associated with inhibition of PP2A. These data suggest that PP2A and GSK-3β function antagonistically to control active zone development, providing a potential mechanism for regulating synaptic efficacy at a single release site.

Introduction

A synapse is composed of an active zone, which is the site of neurotransmitter release site, apposed to a postsynaptic density containing clustered neurotransmitter receptors (Zhai and Bellen, 2004). In *Drosophila*, a neuromuscular junction comprises as many as 500 independent active zones, each directly apposed to a cluster of glutamate receptors (Collins and DiAntonio, 2007). This alignment of presynaptic and postsynaptic specializations is necessary for efficient synaptic transmission. While these hundreds of synapses are formed between the same presynaptic and postsynaptic cell, the strength of these synapses can be regulated independently. For example, when the amount of postsynaptic glutamate receptor is limiting, the remaining receptors preferentially localize opposite the active zones with the highest probability of release (Marrus and DiAntonio, 2004). In addition, the levels of glutamate receptor at individual synapses correlates with amount of the active zone protein Bruchpilot present at each active zone (Marrus and DiAntonio, 2004; Schmid et al., 2008). The levels of Bruchpilot also vary from synapse to synapse. Since Bruchpilot is necessary for both the clustering of calcium channels and the localization of the T-bar release specialization to the active zone (Kittel et al., 2006; Wagh et al., 2006), the differential localization of Brp provides a candidate mechanism for the synapse-specific regulation of synaptic strength. These findings suggest that the formation, maturation, and plasticity of synapses within a single neuromuscular junction may be regulated independently. However, little is known of the signal transduction pathways that control the development of individual synapses. Here we demonstrate that protein phosphatase 2A (PP2A) and glycogen synthase kinase 3β (GSK-3β) function antagonistically to control the development of active zones at individual synapses.

PP2A is one of the cell's major serine-threonine phosphatases. We have shown that the catalytic subunit of PP2A, *microtubule star* (*mts*), and its B' regulatory subunit *well rounded* (*wrd*) are required in the motoneuron for normal synaptic bouton morphology and microtubule structure at the *Drosophila* neuromuscular junction (NMJ) (Viquez et al., 2006). Here, we demonstrate that PP2A activity is also required presynaptically for active zone development—its inhibition leaves many glutamate receptor clusters unapposed to the active zone protein Bruchpilot. This defect in apposition is not due to synaptic retraction in which an entire presynaptic bouton or branch is lost (Eaton et al., 2002). Instead, presynaptic structures such as synaptic vesicles are properly apposed opposite the entire postsynapse and unapposed and apposed glutamate receptors are interspersed within a single synaptic bouton, suggesting that the apposition process is regulated at the level of the individual synapse. Live imaging reveals that these presynaptic defects in active zone development lead to aberrant postsynaptic development, reducing the number of functional synapses. Remarkably, we find that inhibiting a single serine/threonine kinase, the GSK-3β ortholog *shaggy* (Franco et

Received Nov. 21, 2008; revised July 20, 2009; accepted July 27, 2009.

This work was supported by grants from the University of Tübingen (Fortuene 1626-0-0) and from the Landesstiftung Baden-Württemberg to T.M.R. and from the National Institutes of Health (NS043171 and DA020812) to A.D. We acknowledge members of the DiAntonio and Rasse laboratories for helpful discussions, and Howard Wynder, Xiaolu Sun, and Sylvia Johnson for excellent technical assistance.

Correspondence should be addressed to Aaron DiAntonio, Department of Developmental Biology, Campus Box 8103, 660 S. Euclid, Washington University School of Medicine, St. Louis, MO 63110. E-mail: diantonio@wustl.edu.

DOI:10.1523/JNEUROSCI.5584-08.2009

 0270-6474/09/2911484-11$15.00/0

al., 2004), completely suppresses the active zone, microtubule structure, and bouton morphology defects caused by reduced PP2A activity. These findings indicate that regulated phosphorylation via opposing actions of GSK-3β and PP2A is required for both active zone development and synaptic terminal morphology at the *Drosophila* NMJ.

Materials and Methods

Fly stocks. Flies were raised on standard media at 25°C. Wild type flies were of the Canton S line outcrossed to the corresponding Gal4 line for the experiment. The Elav Gal 4 line was used to drive UAS lines panneuronally (Yao and White, 1994). The GeneSwitch elav-Gal4 driver (GS elav) was used to control temporal expression of UAS transgenes in neurons (Osterwalder et al., 2001). To activate the GS elav driver, recently hatched first instar larvae were transferred to soft food with 20 μg/ml RU-486, a nonlethal dose of drug. The *UAS-dnMts* line was obtained from Suzanne Eaton (Max Planck Institute of Molecular Cell Biology and Genetics, Dresden, Germany) and was based on a truncated sequence for the *Drosophila* PP2A catalytic subunit (*mts*) that lacked the catalytic domain (Hannus et al., 2002). The UAS *sgg* A81T line, a transgene for *shaggy* (*sgg*), the *Drosophila* homolog of glycogen synthase kinase-3β, was developed by Marc Bourouis (Université de Nice Sophia Antipolis, Nice, France) and has been shown to act as a dominant negative (Franco et al., 2004). The APC2N175K mutant is a strong loss-of-function allele of *Drosophila* APC2 with a missense mutation converting an invariant asparagine to a lysine (Hamada and Bienz, 2002). The APC2N175K is a strong loss-of-function allelle of *Drosophila* APC2 with a missense mutation converting an invariant asparagine to a lysine (Hamada and Bienz, 2002). The APC1Q8APC2N175K mutant line consists of a recombined chromosome with mutations in both *Drosophila* APC homologs. The APC1 is a loss-of-function allele for *Drosophila* and contains a premature stop codon (Ahmed et al., 1998). The UAS arm S10 line, a transgene for *armadillo (arm*), the *Drosophila* homolog of β catenin, allows for expression of a constitutively active form of β catenin. *Sgg, arm,* and APC alleles were obtained from Bloomington Stock Center (Iowa City, IA).

Immunohistochemistry. Wandering third instar larvae were dissected in ice-cold PBS and fixed in Bouin's fixative for 7 min as previously described (Wu et al., 2005). The following primary antibodies were used: rabbit anti-GluRIII (Marrus et al., 2004), rabbit anti-DVGLUT 1:10,000 (Daniels et al., 2004), mouse anti-Bruchpilot 1:100 (gift from Erich Buchner, Julius-Maximilians-Universität Würzburg, Würzburg, Germany), Cy5-conjugated goat anti-HRP 1:1000 (Jackson Immunoresearch), and mouse α-Futsch 1:100 (mAb 22C10), developed by Seymour Benzer (California Institute of Technology, Pasadena, CA) and obtained from the Developmental Studies Hybridoma Bank, developed under the auspices of the National Institute of Child Health and Human Development and maintained by the Department of Biological Sciences of the University of Iowa (Iowa City, IA). Secondary antibodies Cy3-conjugated goat anti-mouse and Alexa 488 goat anti-rabbit (Jackson Immunoresearch) were used at dilutions of 1:1000.

Imaging and analysis of fixed tissue. Samples were imaged using a Nikon C1 confocal microscope. All imaging was performed on MN 4 1b innervation on anterior segments A2–A3 of muscle 4. For analyses related to numbers of active zones and receptors or degree of microtubule unbundling, each genotype was imaged at the maximum level of brightness while avoiding saturation. For analyses involving relative intensities of NMJ proteins, each genotype was imaged at the same gain. Images were analyzed using MetaMorph software (Universal Imaging). The experimenter was blinded to genotypes during both imaging and analysis. Statistical analysis was performed using one-way ANOVA for comparison of samples within an experimental group. *N* for each condition is described in figures, with a minimum of eight cells from two animals analyzed for a given genotype. All histograms are shown as mean ± SEM.

Unapposed glutamate receptor quantification. To quantify the glutamate receptors unapposed to active zones, wandering third instar larvae were stained with antibodies to Bruchpilot, an active zone marker recognizing the *Drosophila* homolog to CAST (Wagh et al., 2006), DGluRIII, an essential glutamate receptor (Marrus et al., 2004), and HRP, a neuronal membrane marker (Jan and Jan, 1982). The Bruchpilot and DGluRIII antibodies display discrete puncta of active zones and receptors, which can be resolved and counted under high magnification. All three markers were imaged at the maximum gain that avoided saturation. In instances where fainter puncta were observed within an NMJ, two images were taken, a low-gain image that avoided oversaturating brighter staining and a high-gain image which allowed visualization of fainter staining. Blinding to genotypes was maintained throughout imaging and analysis.

Before spot counting, the boundaries of the synaptic terminal were identified based on HRP staining to avoid inclusion of receptors and active zones from innervations other than MN 4 1b. Next, active zone puncta apposed to receptor puncta were counted. An apposed active zone consisted of a Bruchpilot punctum opposite a punctum of glutamate receptor. Infrequent cases of active zones unapposed to glutamate receptors were excluded. Because an active zone punctum is apposed to a single glutamate receptor punctum, glutamate receptor counts were calculated as the number of apposed active zone puncta added to the number of unapposed glutamate receptor puncta. To qualify as an unapposed glutamate receptor, a glutamate receptor spot occurred either in the absence of any nearby active zones or in rare cases had a small area of overlap with an adjacent active zone. Unapposed receptor puncta were divided by total number of receptor puncta to determine the percentage of unapposed glutamate receptors at the NMJ.

Quantification of unapposed receptors at distal and proximal boutons. For this quantification, we included only boutons located (1) near a terminus of the neuromuscular junction or (2) near a nerve immediately preceding the neuromuscular junction.

Distal boutons were considered to be those boutons located within 15 μm of a terminal branch of the NMJ. The starting point for measuring a terminus of a neuromuscular junction was the most distal point of Brp staining. Boutons were excluded from the pool of terminal boutons in the occasional case when they belonged to a very short branch (less than three boutons long). Proximal boutons were those boutons located within 15 μm of a nerve supplying an NMJ. Because many NMJs had multiple branches, numbers for terminal boutons exceeded proximal boutons.

Brp and glutamate receptor puncta within distal and proximal boutons were quantified as described above. Unapposed glutamate receptor amounts were counted for a given set of terminal or proximal boutons, which typically included three boutons. Means for level of unapposed glutamate receptor were calculated by averaging values obtained from sets of distal and proximal boutons. Counts were obtained from eight NMJs for each genotype.

Measurements of axonal trafficking defects. Dissections of wandering third instar larvae were performed as described above, with the brain and axons left intact. Tissue was costained with antibodies to HRP, to delineate axonal outlines, and Brp and DVGlut, as these synaptic proteins are transported along axons. Images were taken of axons at segment A4, using the same gain for all genotypes. Average intensity of Brp and DVGlut over a standard axonal area was measured using MetaMorph.

Futsch unbundling assay. Futsch unbundling was quantified as described previously (Viquez et al., 2006). In brief, larvae were costained with antibodies to Futsch and DVGLUT to label both the cytoskeleton and the cytoplasm of the synaptic terminal, respectively. Futsch staining colocalized with DVGLUT was classified as either unbundled (looped, splayed, or punctate Futsch staining) or bundled Futsch (tightly wound filamentous Futsch staining) (Packard et al., 2002). Futsch staining across genotypes was thresholded to a common value in MetaMorph and areas of unbundled and bundled Futsch were measured. Unbundled Futsch area was divided by total Futsch area as an index of microtubule stability.

Electrophysiology. Intracellular electrophysiological recordings were done as previously reported (Marrus and DiAntonio, 2004). Briefly, wandering third instar larvae were dissected in 0.5 mM Ca Stewart saline (HL3) (Stewart et al., 1994). Both spontaneous miniature excitatory junction potentials (mEJPs) and evoked EJPs were then recorded in 0.5 mM HL3. One-hundred consecutive miniature events were measured per

cell using MiniAnalysis (Synaptosoft) and averaged to determine mean mEJP. Events with a slow rise time course were rejected as artifacts from neighboring electrically coupled muscle cells. To record evoked EJPs, segmental nerves were cut and suctioned into a stimulating electrode, where they received a brief (1 ms) depolarizing pulse. Quantal content was estimated by dividing the mean EJP by the mean mEJP. All cells displayed input resistances >5 MΩ and resting potentials of −60 mV or lower. Statistical analysis was performed using a *t* test to compare pairs of samples or ANOVA for more than two samples in an experimental group.

In vivo *imaging.* Image acquisition for *in vivo* imaging was performed as described (Füger et al., 2007). We used a Zeiss Axiovert 200M microscope equipped with a LSM 510 scanhead (Carl Zeiss) and a Plan-Neofluar ×40 oil 1.3 NA objective (Carl Zeiss). The imaging time series were performed at 25°C. Time points of imaging were 0 and 6 h. The image processing analysis was performed using ImageJ 1.38× (US National Institutes of Health; http://rsb.info.nih.gov./ij/download.html). Image processing was performed as described (Füger et al., 2007). When NMJ regions were enlarged for illustration purposes, the gamma value was adjusted (0.5). The cropped images were rescaled by the factor 2 and a Gaussian blur filtering was applied (pixel radius = 1). Segmentation and quantification was performed as described (Füger et al., 2007). NMJs branches that were oversaturated or that could not be segmented properly were excluded from analysis. To stabilize the variances for *in vivo* imaging data the ratios of new synapses were transformed to logits, i.e., the natural logarithms of the odds. The constant value 0.5 was added to all frequencies such that logarithms of zero were avoided. For the logit-values we compared the groups by a multifactorial ANOVA with the fixed factor group and the random factor animal that is nested under the factor group. The model parameters were estimated according to restricted maximum likelihood (REML). The estimates together with their 95% confidence intervals were back transformed into percentages. We used the statistics package JMP Version 7.0.2.

Electron microscopy. Third instar larvae were dissected in cold calcium free HL3 solution, leaving the body walls and attached musculature. These preparations were fixed overnight at 4°C in a solution of fresh 2% paraformaldehyde, 2.5% glutaraldehyde, 1% tannic acid in 0.1 M cacodylic acid buffer (CB), pH 7.2. Larvae were then unpinned and transferred into 1% OsO_4 in CB for 1 h at room temperature and stained *en bloc* with 1% uranyl acetate in H_2O. The tissue was then dehydrated via an ethanol series followed by incubations in propylene oxide. Next, samples were incubated overnight in a 1:1 mix of propylene oxide in Epon 812 (hard formulation; Ted Pella) under −5 inches Hg vacuum. The next day, the samples were changed into fresh Epon resin for several hours and then placed in fresh Epon in coffin molds. The resin was cured at 60°C for 48 h and sectioned with a diamond knife (Micro Star Technologies) on a Leica EM UC6 ultramicrotome (Leica Microsystems) at 70 nm thickness. Grids were stained with filtered 5% uranyl acetate in methanol for 10 min, washed, dried, and stained for 2 min in filtered lead citrate. Pictures were taken on a Hitashi H-7500 transmission electron microscopy (TEM) using 70 kV accelerating voltage. Image magnifications ranged from 15,000 to 80,000 to allow visualization of structures ranging in size from an entire bouton to a single active zone. Electron micrographs of NMJs were taken from muscles 6–7 and segments A2-A3 in three larvae of each genotype. Images from a total of 53 boutons in wild type (GS Elav Gal 4/+) and 73 boutons from dnPP2A mutants (GS Elav Gal 4/UAS dnMts) were used for analysis. Image files were given random code names to allow blinding to genotype during analysis. MetaMorph imaging software was used to measure bouton circumference and active zone length. Active zones were identified as linear electron densities found between pre-and postsynaptic membranes. High-magnification images (>30,000×) were used to determine the presence of a T-bar, which was defined as an electron dense rod surrounded by vesicles and apposed to the presynaptic membrane. Low-magnification images were used for measurements of bouton circumference while higher-magnification images were used for measurements of active zone length.

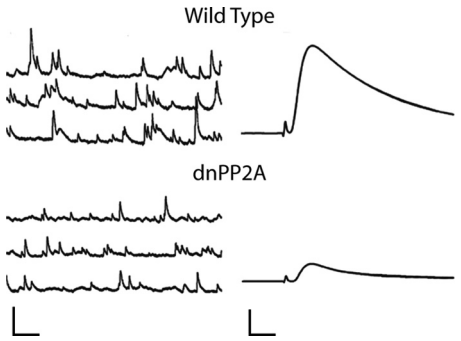

Figure 1. Inhibition of PP2A during development impairs synaptic function. Representative traces of spontaneous miniature EJPs (left) and evoked EJPs (right) for wild type (GS Elav Gal 4/+) and dnPP2A (GS Elav Gal 4/UAS dnMts). Spontaneous miniature potentials in dnPP2A animal are as a group lower than those in wild-type animals. Note the dramatic decrease in size of the average evoked potential in the dnPP2A animal. Calibrations: 500 ms, 2 mV for spontaneous miniature potentials and 12.5 ms, 5 mV for evoked potentials.

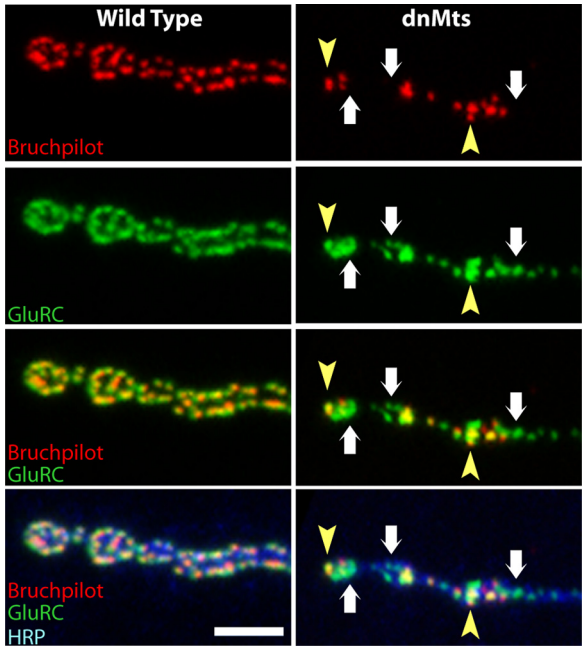

Figure 2. Inhibition of PP2A leads to unapposed glutamate receptors. MN 4 1b innervation of muscle 4 in wild type (GS elav Gal4/+) and dnPP2A (GS elav Gal4/UAS dnMts). Larvae are tripled stained with antibodies to the active zone protein Bruchpilot, the glutamate receptor DGluRIII, and the neural membrane marker HRP. Bruchpilot and glutamate receptor staining colocalize at almost all synpases in wild-type animals. In contrast, dnPP2A animals show both colocalized Bruchpilot and receptors (yellow arrowhead) as well as glutamate receptors unapposed to Bruchpilot (white arrows). Scale bar, 10 μm.

Results

Reduced PP2A activity impairs synaptic function

Previously we demonstrated that PP2A functions in the motoneuron to regulate the growth and morphology of the neuromuscular junction (Viquez et al., 2006). We now investigate whether PP2A also regulates synaptic function at the NMJ. Because PP2A is required for viability (Snaith et al., 1996), we inhibited PP2A activity solely in the nervous system via the Gal 4/UAS system. PP2A activity was reduced using a dominant-negative transgene of the single *Drosophila* PP2A catalytic subunit, *mts* (Hannus et al., 2002; Sathyanarayanan et al., 2004). We expressed this transgene with the neuronal GS elav driver (Osterwalder et al., 2001), whose expression is activated by addition of

the drug RU-486. To avoid disrupting the role of PP2A in initial establishment of the NMJ, we treat larvae with RU-486 as young first instar larvae, a stage at which axons have reached their targets and functional synapses have been established. This protocol successfully circumvents lethality from loss of PP2A activity, as treated animals survive through adulthood. To analyze synaptic function, we performed intracellular recording from muscle 6 of segments A3 and A4 and recorded evoked and spontaneous synaptic potentials from the NMJs of larvae expressing the dnMts transgene under GS elav. We find that PP2A inhibition leads to a dramatic reduction in the synaptic strength (Fig. 1), with a 73% reduction ($p < 0.01$) in the amplitude of evoked EJPs. There is also a 37% reduction ($p < 0.01$) in the amplitude of spontaneous miniature EJPs without a significant decrease in their frequency ($p > 0.4$). The decrease in mEJP amplitude indicates that some of the decrease in synaptic strength is due to impaired postsynaptic response to transmitter. This decrease in mEJP amplitude is likely due to postsynaptic defects, and is associated with a modest decrease in the levels of the essential glutamate receptor subunit DGluRIII (14% decrease, $p < 0.0001$). While this modest decrease in mEJP amplitude accounts for some of the decrease in evoked release, most is due to a presynaptic decrease in the number of vesicles released following an action potential. Quantal content calculated by the direct method (EJP/mEJP) is reduced by 60% ($p < 0.05$, $n = 6$) when PP2A is inhibited. Hence, PP2A is required presynaptically for normal release of transmitter.

Reduced PP2A activity disrupts localization of the active zone protein bruchpilot

To investigate the mechanism of synaptic dysfunction following PP2A inhibition, we analyzed synaptic structure in these larvae. Our previous analysis demonstrated that PP2A is required for the normal morphology of synaptic boutons. This is not, however, an adequate explanation for functional defects, since transmitter release and reception does not occur at the level of the bouton. Instead, each bouton comprises many individual active zones, each of which is apposed to a cluster of postsynaptic glutamate receptor clusters. This active zone/receptor cluster pair is the functional synaptic unit. We stained larvae with an antibody to Bruchpilot (Brp), the *Drosophila* homolog of CAST, which marks active zones (Wagh et al., 2006), and an antibody to the essential glutamate receptor subunit, DGluRIII (Marrus et al., 2004). We limited our quantitative analysis to the identified glutamatergic MN 4 1b innervation at anterior segments of muscle 4 in wandering third instar larvae, although similar effects were observed at all type 1 glutamatergic synapses. At synapses from wild-type larvae treated with RU-486, Brp and DGlurRIII are almost always in perfect apposition (Fig. 2). When PP2A is inhibited, there is an ~30% reduction in the number of Brp puncta (*GSelav/+*: 267 ± 9; *GSelav/UAS-dnMts*: 198 ± 20, $p < 0.01$). However there is no significant change in the number of glutamate receptor clusters (*GSelav/+*: 267 ± 9; *GSelav/UAS-dnMts*: 279 ± 23, $p > 0.05$). Hence, this loss of Brp clusters disrupts the normally precise apposition of Brp and GluR, leaving ~30% of postsynaptic glutamate receptor clusters unapposed to a Brp puncta (Fig. 2) (% GluR unapposed: *GSelav/+*: 0.1% ± 0.1%; *GSelav/UAS-dnMts*: 29.5% ± 3.4%, $n = 16$ nmjs, $p < 0.001$).

Since PP2A is an essential gene, our analysis of its role in synaptic development relies on the tissue-specific expression of a dominant-negative transgene, *UAS-dnMts*. This transgene has been shown to reduce PP2A activity in a number of systems (Hannus et al., 2002; Sathyanarayanan et al., 2004). To test whether *UAS-dnMts* is acting as a dominant-negative in this system, we performed the classic genetic test for a dominant negative by removing a wild type copy of the *mts* gene and assaying for enhancement of the phenotype. In *Drosophila*, *mts* heterozytotes exhibit a 30% reduction in PP2A activity based on phosphorylation assays (Snaith et al., 1996). We generated flies expressing the *dnMts* transgene in the presence of one mutant *mts* chromosome. To facilitate our capacity to observe enhancement, we drove the *dnMTS* transgene with a weaker Gal4 driver. In an otherwise wild type background removing one copy of *mts* does not lead to a significant increase in the percentage of unapposed glutamate receptors (supplemental Fig. 1, available at www.jneurosci.org as supplemental material). However, the *mts* heterozygote enhances the *dnMts* phenotype, leading to an additional 30% increase in the proportion of unapposed receptors ($p < 0.05$). This enhancement is consistent with the function of *UAS-dnMts* as a dominant negative, and confirms that PP2A activity is required for the apposition of normal active zones opposite glutamate receptors.

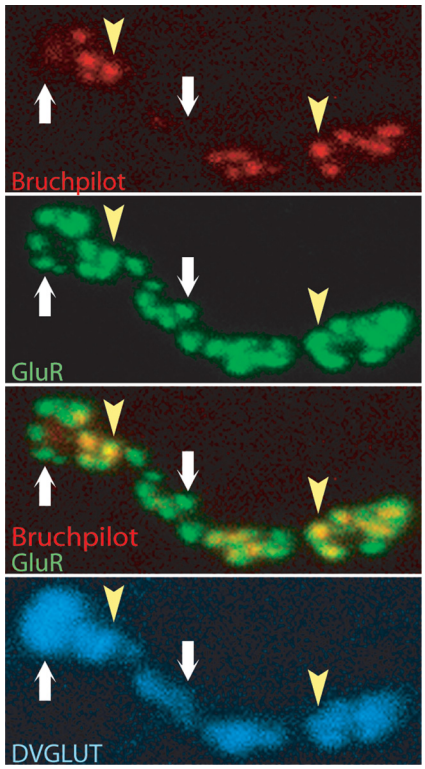

Figure 3. Inhibition of PP2A does not induce synaptic retraction. A terminal branch of MN 4 1b is shown from a dnPP2A (G Selav Gal 4/UAS dnMts) larvae triple labeled with antibodies to the synaptic vesicle protein DVGLUT, Bruchpilot, and DGluRIII. DVGLUT staining is present throughout the nerve terminal, indicating that the presynaptic terminal is not retracted. Note that glutamate receptors apposed to Bruchpilot (yellow arrowheads) and unapposed to Bruchpilot (white arrows) are present in a salt-and-pepper pattern throughout the terminal, which is not consistent with the distal-to-proximal loss of the presynaptic terminal observed with synaptic retraction.

Unapposed glutamate receptor clusters preferentially occur at the distal NMJ

The presence of unapposed receptors could reflect defects in the maturation or maintenance of active zones. One mechanism that can lead to unapposed receptors is the failure to maintain entire nerve branches leading to nerve terminal retraction. At the *Drosophila* NMJ, retraction is assayed by costaining for presynaptic and postsynaptic proteins, and identifying regions where postsynaptic proteins including receptors are unapposed

to presynaptic structures such as synaptic vesicles (Eaton et al., 2002). To investigate whether unapposed glutamate receptors arise from retraction when PP2A is inhibited, we analyzed synaptic morphology in larvae triple-stained with antibodies to active zones, glutamate receptor, and the synaptic vesicle protein DVGLUT. Nerve terminal retraction occurs in a distal to proximal manner, so we focused on unapposed glutamate receptors occurring near terminal boutons (Fig. 3). Numerous glutamate receptor clusters are unapposed to Brp; however, DVGLUT staining is present, including at the terminal bouton itself. Furthermore, unapposed glutamate receptors alternate with apposed glutamate receptors at multiple points along the NMJ, including within a single bouton, a finding inconsistent with a continuous retraction of the nerve. Instead, synaptic vesicles are distributed normally and properly apposed Brp and GluR clusters can occur throughout the NMJ. Hence, the defect is not due to a failure to maintain the nerve terminal.

While unapposed receptors can occur throughout the NMJ, we noticed that the proportion of unapposed receptors appeared to be higher in more distal regions of the nerve terminal. This is interesting because new synaptic boutons tend to be added at the periphery of the synaptic tree (Zito et al., 1999), suggesting that PP2A inhibition might affect the maturation of newly formed synapses rather than the maintenance of previously formed synapses. We quantified the fraction of unapposed receptors in both the proximal 15 μm of NMJ and the distal-most 15 μm of each synaptic branch and found an approximately fivefold increase in the proportion of unapposed receptors in the distal regions of the NMJ (Fig. 4). As a second test of this hypothesis, we began expressing the dominant-negative PP2A transgene later in development, during the second larval instar, after many more synapses had formed. Later expression of the dnPP2A transgene leads to fewer unapposed receptors, and the vast majority of these aberrant synapses occur in the most distal part of the synaptic tree (Fig. 4*B*,*D*). Without live imaging, it is not possible to know when any particular synapse formed; however, the finding that the late inhibition of PP2A preferentially affects the distal part of the NMJ where new synapses tend to form is consistent with the model that PP2A is required for the maturation rather than maintenance of active zones.

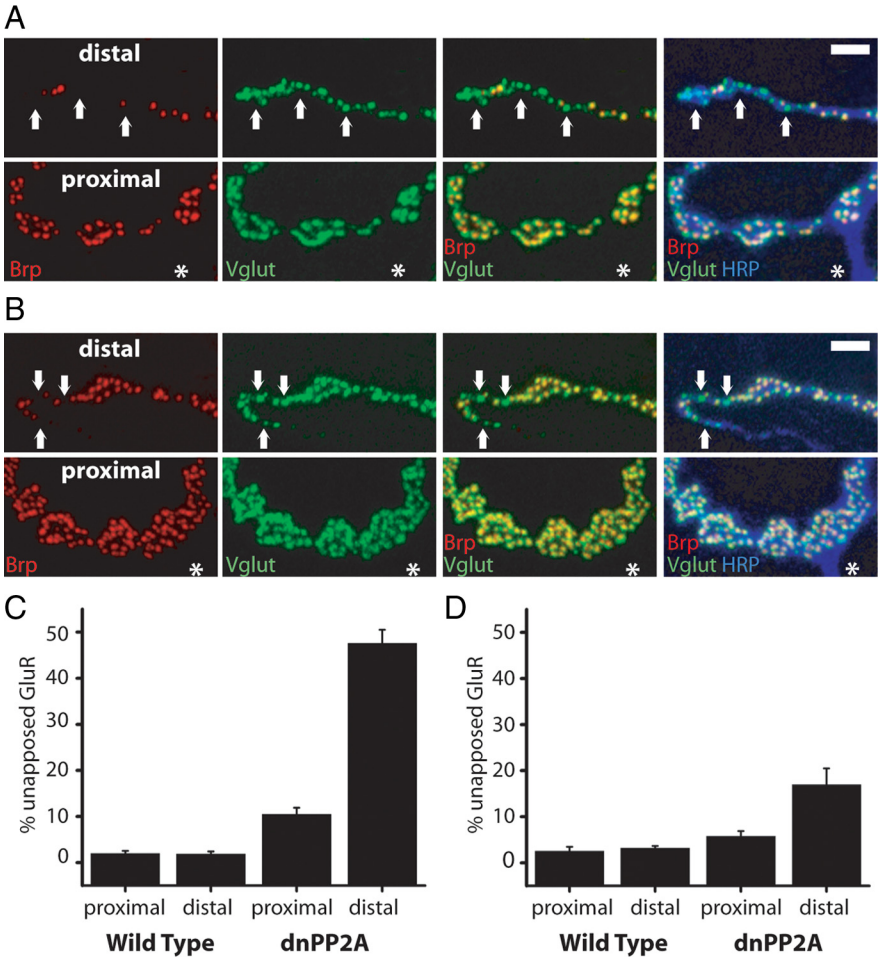

Figure 4. Unapposed glutamate receptors are most prevalent at the distal NMJ. ***A***, Boutons from third instar larvae with UAS dnMts driven since the first instar stage (GS Elav-Gal 4/UAS-dnMts). Boutons are costained with antibodies to Brp, DGluRIII, and HRP. Upper panels show a terminal NMJ branch, which is the region of the NMJ where new synapses tend to be added. White arrows highlighting several areas of glutamate receptor unapposed to Brp. The lower panel shows proximal boutons, with an asterisk indicating the adjoining nerve. In contrast to distal boutons, the active zones and receptors in the proximal boutons are primarily apposed. Scale bar, 5 μm. ***B***, Boutons from third instar larvae with UAS dnPP2A driven since the second instar stage (GS Elav Gal4/UAS dnMts). Antibody staining and layout of images is as above. In the terminal branch in the top panels, white arrows indicate several sites of glutamate receptors unapposed to Brp. Proximal boutons show uniform apposition of Brp and DGluRIII. Asterisk indicates adjoining nerve. Scale bar, 5 μm. ***C***, Quantification of unapposed glutamate receptors at proximal and distal boutons in wild-type (WT; GS Elav Gal 4/+) and dnPP2A animals driven by GS Elav Gal 4 since first instars. Wild-type animals show negligible unapposed glutamate receptors. The level of unapposed glutamate receptors at proximal boutons in dnPP2A animals, 10%, is not significantly different from wild type ($p > 0.4$). The level of unapposed glutamate receptors at distal boutons in dnPP2A animals, 48%, differs significantly from distal wild-type boutons ($p \ll 0.001$) and proximal dnPP2A boutons ($p \ll 0.001$). $N = 12$ for WT proximal, $N = 21$ for WT distal, $N = 23$ for dnPP2A proximal, and $N = 47$ for dnPP2A distal. ***D***, Quantification of unapposed glutamate receptors at proximal and distal boutons in wild type (GS Elav Gal 4/+) and dnPP2A animals driven by GS Elav Gal 4 since second instars. Wild-type animals show negligible unapposed glutamate receptors. The level of unapposed glutamate receptors at proximal boutons in dnPP2A animals, 6%, is not significantly different from wild type ($p > 0.95$). The level of unapposed glutamate receptors at distal boutons in dnPP2A animals, 17%, differs significantly from levels in distal wild-type boutons ($p < 0.001$) and proximal dnPP2A boutons ($p < 0.05$). $N = 12$ for WT proximal, $N = 25$ for WT distal, $N = 11$ for dnPP2A proximal, and $N = 29$ for dnPP2A distal.

Inhibiting PP2A leads to a decrease in synaptic density

Bruchpilot is required for the active zone localization of T-bars, electron dense specializations that likely promote transmitter release (Kittel et al., 2006). Since Bruchpilot localization is disrupted when PP2A is inhibited, we investigated whether T-bar localization to the active zone was similarly affected. We performed an ultrastructural analysis of type 1b boutons at the NMJ on muscles 6 and 7 in wild-type and PP2A inhibited larvae (Fig. 5; Table 1). Active zones were identified as sites where tightly apposed presynaptic and postsynaptic membranes are separated by a region of increased electron density. We measured bouton circumference, active zone number, active length, and the presence of T-bars in each genotype (Table 1). Bouton circumference is unchanged in the mutant while active zones are slightly longer

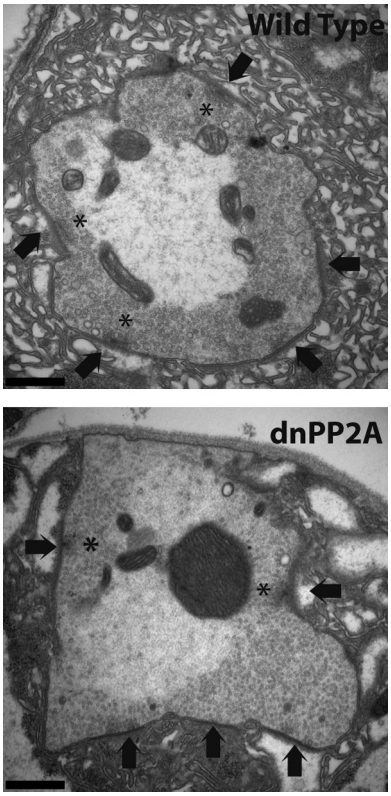

Figure 5. Ultrastructural analysis demonstrates decreased active zone density when PP2A is inhibited. TEM of a Type 1 bouton from wild-type (GS elav Gal 4/+) and dnPP2A (GS elav Gal 4/UAS dnMts) animals. Arrows indicate active zones present in these boutons. Both boutons demonstrate examples of active zones with T-bars (asterisks). Scale bar, 500 nm.

Table 1. Ultrastructural bouton measurements

	Wild type (CS * GSelav)	dnPP2A (WAS dnPP2A * GSelav)	*p* value
Active zone length (nm)	662.5 ± 15.7	728.7 ± 19.5	$p < 0.01$
T bars/active zone	0.413 ± 0.30	0.442 ± 0.041	$p > 0.2$
Active zone density (% az length/bouton length)	34.8 ± 1.6	24.2 ± 1.4	$p \ll 0.001$
Vesicle density (number vesicles/μm^2)	180.2 ± 18.3	110.7 ± 10.2	$p < 0.001$
Mitochondria/area in μm^2	0.790 ± 0.077	0.601 ± 0.093	$p > 0.2$
Bouton circumference	7546 ± 471	8827 ± 574	$p > 0.2$

az, Active zone.

than in wild type (Table 1) ($p < 0.01$). To our surprise, however, there is no difference in the proportion of active zones with T-bars in the two genotypes (Table 1) ($p > 0.2$). There is, however, a 31% decrease in the density of active zones when PP2A is inhibited (Table 1) ($p < 0.001$). This decrease in active zone density seen in electron micrographs is consistent with the decrease in the number of Brp puncta observed in the confocal analysis (Fig. 2). These data support the model that fewer active zones form when PP2A is inhibited, but that those active zones that do form still have Bruchpilot, and hence T-bars.

Synaptic boutons are often densely packed with synaptic vesicles and mitochondria. In the mutant, however, we often observed boutons in which the interior appeared to be less full of synaptic material. To investigate this observation, we quantified the density of synaptic vesicles and mitochondria in the synaptic terminal (Table 1). There is a decrease in the density of synaptic vesicles in the mutant nerve terminals (38% decrease, $p < 0.001$) as well as a trend toward a decrease in the density of mitochondria. As an independent test of this observation we stained for the synaptic vesicle marker DVGLUT and observed a 33% decrease ($p \ll 0.001$) across the NMJ. Hence, the number of synaptic vesicles and the density of a vesicle protein are both reduced in the mutant.

Live imaging of glutamate receptor clustering

The decrease in both active zone density and Brp puncta implies that the glutamate receptor clusters unapposed to Brp puncta may be unapposed to active zones. The clustering of GluRs requires the motoneuron (Broadie and Bate, 1993), and so the presence of receptor clusters without adjacent active zones is surprising. To investigate whether these receptors cluster normally, we measured the size of apposed and unapposed GluR clusters. In wild type, the average GluR cluster is 0.37 μm^2. With inhibition of PP2A, the average size of GluR clusters that are apposed to Brp puncta is 0.62 μm^2. This increase in GluR cluster size is consistent with the increased active zone length measured in the electron micrographs. In contrast, the GluR clusters that are unapposed to Brp puncta are very small, with an average size of 0.23 μm^2. This suggests a defect in the formation or maintenance of unapposed GluR clusters.

To investigate the dynamics of GluR clustering, we performed live imaging of GFP-tagged glutamate receptors (Rasse et al., 2005) in both wild-type and PP2A inhibited larvae. Third instar larvae expressing GFP-DGluRIIA were imaged, allowed to develop for an additional 6 h, and then imaged again (Fig. 6). Receptor clusters that had been previously imaged were identified and both gain and loss of receptor clusters was quantified. We find an approximately threefold decrease in the proportion of newly formed receptor clusters when PP2A is inhibited (Fig. 6) ($p < 0.05$). During this time window a small proportion of GluR clusters are lost in both genotypes. Hence, during these 6 h of development there is very little net synapse addition in the mutant compared with wild type. Therefore, the defects in active zone development caused by the presynaptic inhibition of PP2A also lead to inappropriate postsynaptic development.

GSK-3β, a serine-threonine kinase, works in opposition to PP2A

PP2A's likely role in synaptic development prompted us to screen for other signaling molecules that could interact with PP2A to mediate this role. We tested for genetic interactions between PP2A and molecules known to interact with PP2A during development. One of these molecules, *Drosophila* APC2 (McCartney et al., 1999), an ortholog of the adenomatous polyposis coli protein (APC), enhances the PP2A synaptic phenotype. PP2A can bind and dephosphorylate APC, and both work together in a number of pathways. Heterozygous APC2 mutations do not lead to unapposed GluR clusters in an otherwise wild-type background. However, APC2 heterozygotes enhance the PP2A phenotype, leading to an approximate doubling of the proportion of unapposed GluR clusters (supplemental Fig. 2, available at www.jneurosci.org as supplemental material). This suggests that APC2 may potentiate PP2A function during synaptic development, which is consistent with their complementary roles in other systems.

PP2A's genetic interaction with APC, a prominent signaling molecule, supports the hypothesis that PP2A's function is mediated via developmental signaling pathways. The inhibition of PP2A is expected to lead to the hyperphosphorylation of substrates due to the unopposed action of a serine threonine kinase

or kinases. We reasoned that inhibition of the relevant kinase should suppress the PP2A synaptic phenotype. We tested for a genetic interaction between PP2A and the serine-threonine kinase glycogen synthase kinase-3β, since it shares substrates with PP2A including APC (Ikeda et al., 2000). GSK-3β is an essential gene, and hypomorphs in *shaggy*, the *Drosophila* GSK-3β homolog, display decreased body size and thin muscles (N. Viquez and A. DiAntonio, unpublished observations). To test for an effect of reduced GSK-3β activity while circumventing generalized larval defects, we used a tissue-specific kinase dead transgene of *shaggy*, which acts as a dominant negative (Bourouis, 2002; Franco et al., 2004). We expressed this transgene in the nervous system together with the *dnMts* to allow simultaneous reduction of GSK-3β and PP2A activity. Figure 7 shows representative boutons from wild-type larvae, larvae with reduced PP2A or reduced GSK-3β activity, or larvae with reduction of both PP2A and GSK-3β activity. When GSK-3β is inhibited in an otherwise wild-type background, glutamate receptors cluster opposite Brp puncta normally. However, simultaneously reducing GSK-3β and PP2A activity leads to a dramatic suppression of the PP2A phenotype, with levels of unapposed glutamate receptors dropping to near wild-type levels (Fig. 7). This suppression does not result from a dilution of *UAS-dnMts* expression, as combination of *UAS-dnMts* with an additional UAS transgene fails to suppress the *dnMts* phenotype (supplemental Fig. 3, available at www.jneurosci.org as supplemental material). Suppression of unapposed glutamate receptors by inhibition of GSK-3β suggests that this single kinase is responsible for coregulating the phosphorylation of PP2A substrate(s) that are required for normal active zone development.

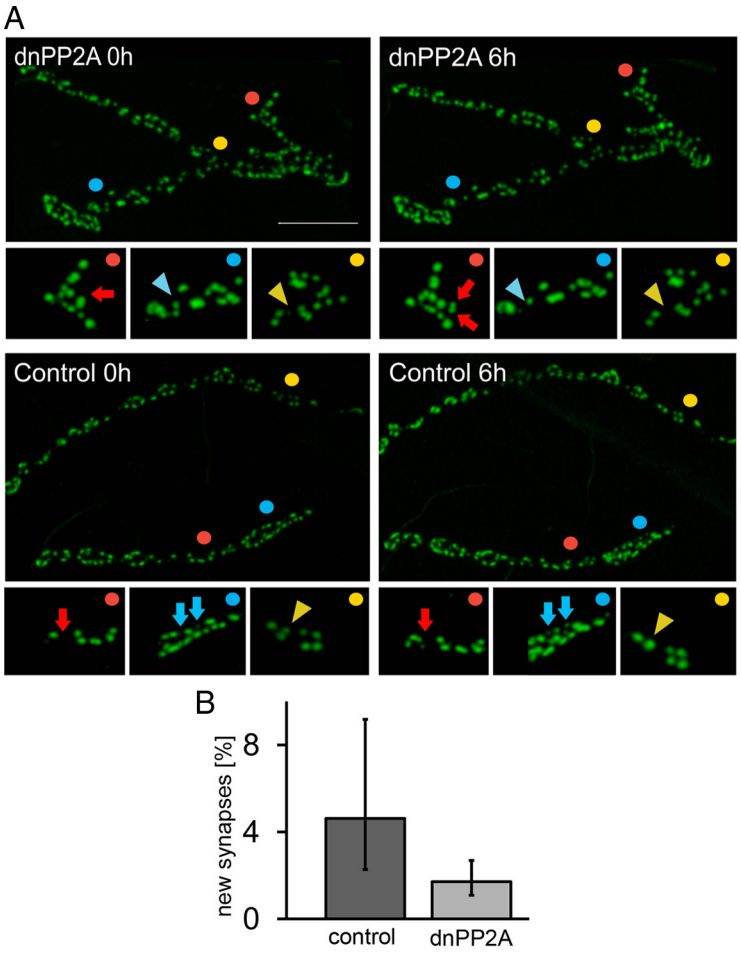

Figure 6. *In vivo* imaging reveals defects in synapse formation when PP2A is inhibited. ***A***, *In vivo* imaging of GFP-labeled DGluRIIA at larval NMJs. Shown are two time points of imaging (0 and 6 h) of individual NMJs from (top) a larvae in which PP2A is inhibited (dnPP2A: DGluRIIa-GFP/+;elav-Gal4/UAS-dnMts) and (bottom) a control larvae (control: DGluRIIA-GFP/+;elav-Gal4/+). Regions of formation and loss of synapses within the NMJs are marked. Enlargements of the areas marked in the upper panel by color-coded dots are shown in the lower panel. New synapses are marked with arrows, lost synapses are marked with arrowheads. Scale bar: 5 μm. ***B***, Quantification of synapse formation. Thirteen control junctions (from 5 different larvae) were compared with forty-two mutant junctions (from 13 different larvae). $p < 0.05$. Error bars equal SEM.

Defects in the axonal transport of active zone components such as Brp to the terminal is a potential mechanism for the aberrant active zone development in these mutants. At the *Drosophila* NMJ, many axon transport mutants (Hurd and Saxton, 1996) show an accumulation of synaptic material in the axon. We find that inhibition of PP2A in the motoneuron results in an accumulation of both the active zone component Brp as well as the synaptic vesicle protein DVGLUT in the axon (supplemental Fig. 4, available at www.jneurosci.org as supplemental material). The accumulation of DVGLUT in the axon is consistent with the decreased levels of synaptic vesicles in nerve terminal. These findings indicate that PP2A is likely required for efficient axonal transport. If transport defects are responsible for the active zone defects, then they should also be suppressed by inhibition of GSK-3β. However, simultaneous inhibition of PP2A and GSK-3β does not suppress the accumulation of synaptic material in the axon, instead the double mutant accumulates more Brp in axons (supplemental Fig. 4, available at www.jneurosci.org as supplemental material). Although Brp continues to accumulate in the axons of the double mutants, the levels of Brp at the NMJ are fully suppressed (average Brp levels at NMJ in arbitrary units: *elavGal4/+* 55 ± 2; *elavGal4/UAS-dnMts* ± 1; *elavGal4/UAS-dnSgg* 54 ± 3; *elavGal4/UAS-dnMts,UAS-dnSgg* 53 ± 3; $p \ll 0.001$ for inhibition of PP2A). These findings genetically separate the active zone development and axon transport defects of the PP2A mutant, and demonstrate that the active zone defect is not secondary to impaired axonal transport.

Defects in both axon transport and active zone development would be predicted to impair efficient transmitter release. To determine which is responsible for the defects in synaptic release seen with inhibition of PP2A, we recorded spontaneous and evoked excitatory junctional potentials and calculated quantal content from third instar larvae in the four genotypes described above. As with axon transport, simultaneous inhibition of PP2A and GSK-3β does not suppress the defects in evoked transmitter release (quantal content: *elavGal4/+* 22.4 ± 2.0; *elavGal4/UAS-dnMts* 10.0 ± 1.6; *elavGal4/UAS-dnSgg* 23.1 ± 1.8; *elavGal4/UAS-dnMts,UAS-dnSgg* 8.9 ± 1.3; $p < 0.001$ for inhibition of PP2A vs control and $p > 0.6$ for inhibition of PP2A vs inhibition

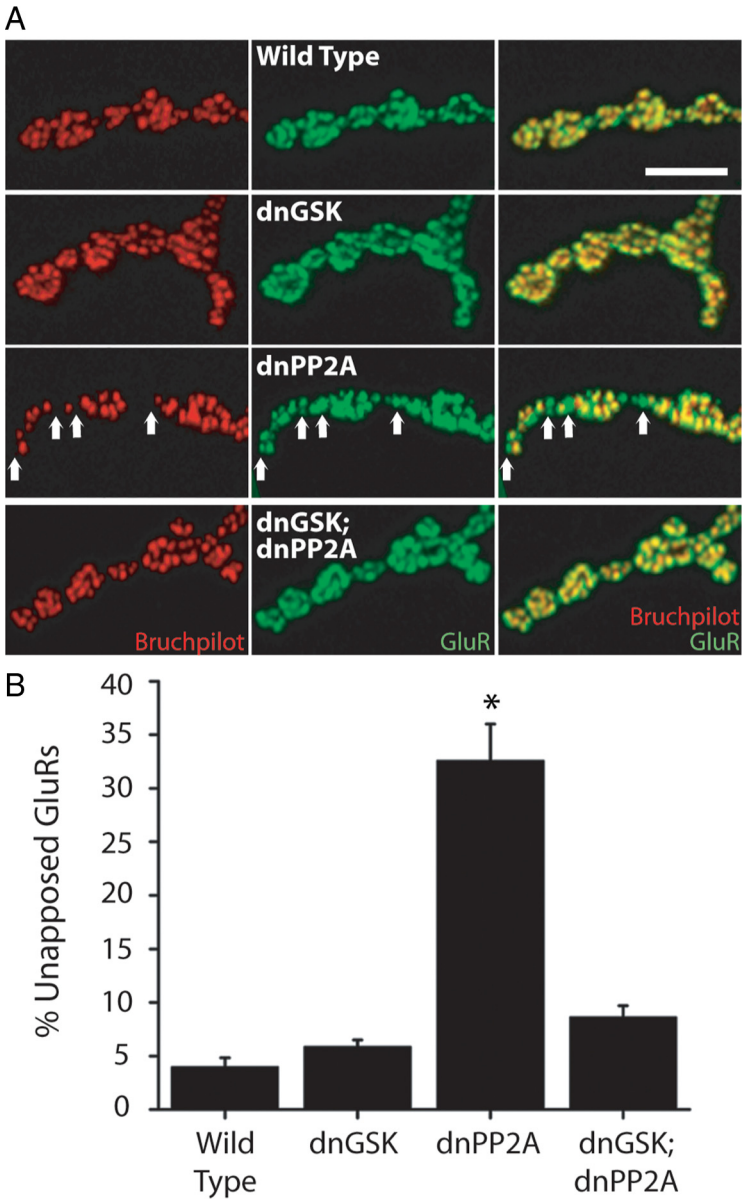

Figure 7. Inhibition of GSK-3β suppresses synaptic apposition defects due to PP2A inhibition. ***A***, A terminal branch from MN 4 1b innervation is shown costained with antibodies to Bruchpilot and DGluRIII from wild-type (Elav Gal 4/+), dnGSK (UAS dnGSK-3β/+; Elav Gal 4/+), dnPP2A (Elav Gal 4/UAS dnMts), and dnGSK; dnPP2A (Elav Gal 4/UAS dnGSK-3β; UAS dnMts/+) larvae. White arrows illustrate unapposed glutamate receptors in dnMts. For all other genotypes, colocalization of Bruchpilot and receptors appears essentially as in wild-type animals. Scale bar, 7 μm. ***B***, Quantification is shown of the percentage of unapposed glutamate receptors. Levels of unapposed glutamate receptors are not significantly different among wild type, dnGSK-3β, and dnGSK-3β; dnMts ($p > 0.9$). Unapposed glutamate receptors are increased by >700% relative to wild type in Elav dnMts, *$p < 0.01$. $N = 8$ for all genotypes. Error bars equal SEM.

of PP2A and GSK-3β). The continued defect in evoked release suggests that either impaired axon transport is the major cause of decreased transmitter release or that the active zones formed while both PP2A and GSK-3β are inhibited may be functionally impaired.

GSK-3β inhibition suppresses cytoskeletal destabilization induced by PP2A inhibition

In addition to PP2A's role in regulating synaptic development, we have previously demonstrated PP2A activity regulates cytoskeletal structure and synaptic terminal morphology at the NMJ. Reduction of PP2A activity leads to increased unbundling of the microtubule associated protein Futsch, a feature correlated with instability of microtubules (Fig. 8*A*). GSK-3β has been implicated in the regulation of microtubule dynamics in axon outgrowth and at the *Drosophila* NMJ (Franco et al., 2004; Gögel et al., 2006; Ataman et al., 2008). To ask whether GSK-3β could also suppress the PP2A cytoskeletal phenotype, we reexamined the genetic interaction of PP2A and GSK-3β by analyzing the percentage of unbundled Futsch present at the NMJ. Neuronal inhibition of PP2A led to 46% unbundled Futsch relative to 25% unbundled Futsch in wild-type animals (Fig. 8*B*). Reduction of GSK-3β activity alone revealed a small but statistically insignificant increase in unbundled Futsch levels. Concomitant reduction of PP2A and GSK-3β activity results in NMJs with wild-type levels of unbundled Futsch, and in the restoration of the normal synaptic terminal branching and bouton morphology (Fig. 8*A*). Hence, reduced GSK-3β suppresses the cytoskeletal destabilization incurred by reduced PP2A activity. In addition, we previously demonstrated that loss of the PP2A regulatory subunit *wrd* leads to a significant increase in the size of boutons (Viquez et al., 2006), a phenotype that is also suppressed by inhibiting GSK-3β (25% decrease in bouton size, $p < 0.01$). Hence, reducing GSK-3β not only suppresses the effects of PP2A on the development of the active zone/glutamate receptor synaptic dyad, but also on cytoskeletal structure and bouton morphology of the NMJ. These findings demonstrate that GSK-3β and PP2A work as an antagonistic kinase/phosphatase pair to regulate multiple aspects of synaptic development.

Discussion

Here we demonstrate that the serine-threonine phosphatase PP2A is required in the presynaptic neuron for normal development and maturation of presynaptic release sites. This action of PP2A is opposed by the serine-threonine kinase GSK-3β, suggesting that this phosphatase/kinase pair coregulate the phosphorylation state and activity of proteins that are required for proper synaptic development.

The role of PP2A for synaptic development

At the *Drosophila* NMJ, the synaptic terminal of a motoneuron is a branched chain of synaptic boutons whose gross structure is strongly influenced by the cytoskeleton. Within each synaptic terminal, there are hundreds of individual synapses, neurotransmitter release sites with an active zone directly apposed to a cluster of postsynaptic glutamate receptors. Most studies in *Drosophila* have focused on genes controlling synaptic terminal develop-

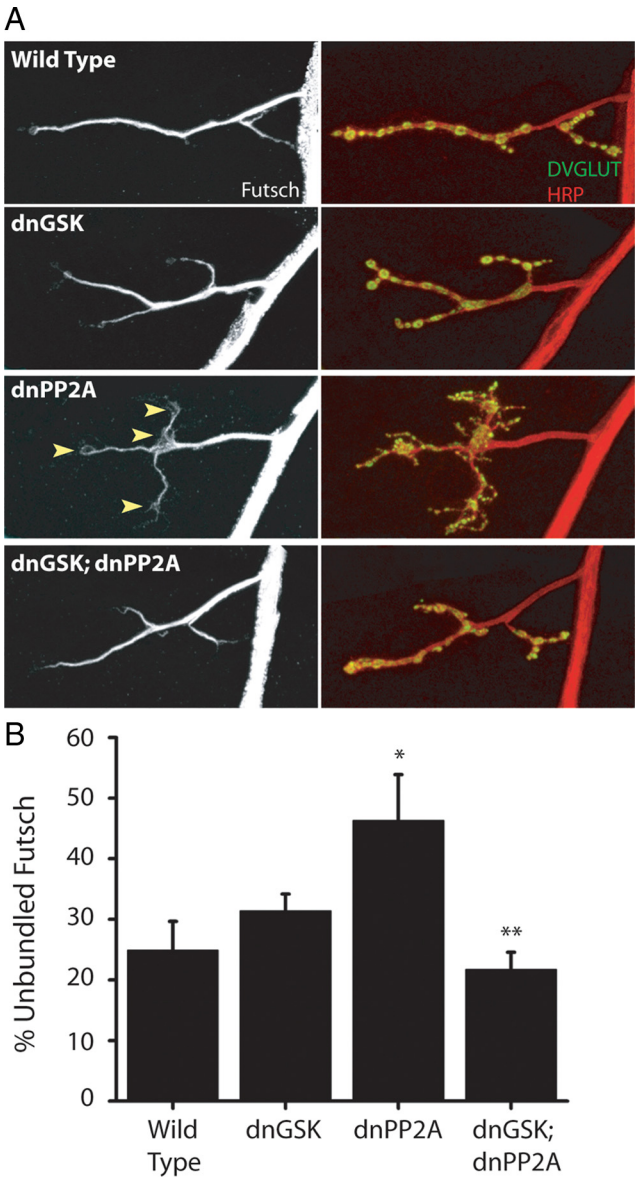

Figure 8. Inhibition of GSK-3β suppresses cytoskeletal and synaptic terminal morphology defects induced by inhibition of PP2A. ***A***, Representative MN 4 1b NMJs are shown for wild-type (Elav Gal 4/+), dnGSK (UAS dnGSK-3β/+; Elav Gal 4/+), dnPP2A (Elav Gal 4/UAS dnMts), and dnGSK; dnPP2A (UAS dnGSK3-β, Elav Gal 4/UAS dnMts) larvae. NMJs are stained with antibodies to Futsch (left panels) and DVGLUT and HRP (right panels). Note increased Futsch unbundling marked by arrowheads in Elav dnPP2A genotype. Note also that the aberrant synaptic terminal morphology induced by inhibition of PP2A is suppressed by inhibition of GSK-3β. ***B***, Quantification of mean percentage unbundled Futsch at the NMJ. Levels of unbundled Futsch in dnGSK-3β and dnGSK-3β; dnPP2A are not significantly different from wild type $p > 0.3$, and $p > 0.5$, respectively. dnPP2A demonstrates an 86% increase in unbundled Futsch relative to wild type, $^{*}p < 0.05$. Levels of unbundled Futsch in dnGSK-3β, dnPP2A are reduced by 53% from dn PP2A, $^{**}p < 0.01$. $N = 8$ for all genotypes. Error bars equal SEM.

ment (Collins and DiAntonio, 2007). However, with the recent development of antibodies to the active zone component Bruchpilot and the essential glutamate receptor DGluRIII, a genetic analysis of active zone and postsynaptic density development is now feasible (Wairkar et al., 2009). In our previous studies we demonstrated that PP2A acts in the motoneuron to control synaptic terminal morphology likely via regulation of microtubules. Here, we demonstrate that PP2A is also essential for the proper development of the individual synaptic unit, the active zone, and glutamate receptor dyad.

Presynaptic inhibition of PP2A impairs synaptic transmission, leading to a large decrease in quantal content. While investigating potential morphological explanations for defective transmitter release, we observed that many glutamate receptor clusters are unapposed to the active zone protein Bruchpilot. This is not due to retraction of the presynaptic terminal, since apposed and unapposed GluR clusters are intermingled throughout the terminal in a salt and pepper pattern, and presynaptic structures such as synaptic vesicles are still apposed to the entire extent of the postsynaptic specialization. Instead, there is a defect at the level of the individual synapse. These GluR clusters may be unapposed to active zones, or may be apposed to abnormal active zones lacking Bruchpilot. Two lines of evidence suggest that these GluR clusters may be unapposed to active zones. First, Bruchpilot is required for the localization of T-bars to the active zone, so if many active zones are missing Bruchpilot, then there should be a decrease in the proportion of active zones with T-bars. However, when PP2A is inhibited we see no change in the proportion of active zones with T-bars. Second, with PP2A inhibition the number of Brp puncta is down, as is the density of active zones as defined by ultrastructural analysis. This suggests that there is not a large pool of active zones without Brp. Both of these findings suggest that there are fewer active zones, and that those active zones that form do contain Brp. If this is so, then why are GluR clusters present that are unapposed to active zones? This could be due either to a problem with synapse formation/maturation or maintenance. While we do not know which is the case, we prefer that model that there is a defect in the formation or maturation for the following reasons. First, unapposed receptors are more prevalent in the distal regions of the NMJ where new synapses tend to be added. Second, the unapposed receptors form quite small clusters, while newly forming GluR clusters in wild type are also quite small (Rasse et al., 2005). Finally, live imaging reveals that fewer GluR clusters form late in larval development, demonstrating a defect in synapse formation.

We propose a model in which PP2A activity is required for the maturation phase of synapse development. In this view, at a wild-type synapse a signal would initiate synapse formation, leading to postsynaptic clustering of glutamate receptors as well as transsynaptic interactions that form the tightly apposed presynaptic and postsynaptic membranes as seen in electron micrographs. Later, additional active zone components such as Brp would be recruited to the active zone, a process known to occur after GluR clustering (Rasse et al., 2005). With PP2A inhibition, this unknown signal would still initiate synapse formation and induce GluR clusters. However, at some fraction of nascent synapses the maturation process would fail. The GluR clusters could be trapped in their small, immature state or lost, while the transsynaptic process leading to the tight apposition of presynaptic and postsynaptic membranes would also fail and Brp would not be recruited. We cannot, however, rule out the alternate model that synaptic maintenance is disrupted, and that unapposed GluR clusters are the remains of synapses at which the presynaptic terminal has been lost. Regardless of the precise mechanism, these data demonstrate that PP2A is required to ensure the correct apposition of structurally normal active zones and glutamate receptors at the synapse.

PP2A and GSK-3β function antagonistically to control synapse development

PP2A is one of the major serine/threonine phosphatases in the cell, so inhibiting its function likely leads to hyperphosphorylation of many proteins (Janssens and Goris, 2001). Hence, pheno-

types could be due to the pleiotropic effects of misregulating numerous pathways. Our data, however, argue for a good deal of specificity in the function of PP2A for the synaptic morphology phenotypes we assayed. Inhibiting PP2A in the neuron leads to misapposed GluR clusters, a disrupted synaptic cytoskeleton, and an altered bouton morphology. Each of these phenotypes is suppressed when GSK-3β is inhibited. This suggests that these synaptic phenotypes are due to the misregulation of a pathway that is antagonistically regulated by PP2A and GSK-3β. We do not, however, see opposite phenotypes when PP2A is overexpressed, suggesting that hyperphosphorylation affects this pathway more than hypophosphorylation. While genetic studies cannot prove that this phosphatase/kinase pair act directly on the same substrate, the simplest interpretation of the data is that PP2A and GSK-3β coregulate the phosphorylation state and activity of a protein or proteins that are required for the proper development of active zones and the synaptic cytoskeleton. While these PP2A phenotypes are all suppressed by inhibition of GSK-3β, there is no suppression of the accumulation of synaptic material in the axon, a phenotype consistent with defects in axonal transport (Hurd and Saxton, 1996). Decreased transport of active zone material such as Brp is a plausible mechanism for the active zone defects in this mutant. However, the failure of GSK-3β inhibition to suppress the axonal transport phenotype demonstrates that the active zone maturation and axon transport phenotypes are genetically separable. Hence, the accumulation of Brp in the axon cannot be responsible for the defects in synaptic maturation.

We do not know the identity of the pathway regulated by PP2A and GSK-3β. One candidate substrate is APC2, which binds to and stabilizes the plus end of microtubules and which is a characterized substrate of both PP2A and GSK-3β (Ikeda et al., 2000; Barth et al., 2008). In hippocampal cells phosphorylation of APC by GSK-3β inhibits APC function and so disrupts microtubule stability and axon outgrowth (Zhou et al., 2004). We show that loss of APC2 dominantly enhances the PP2A phenotype, which is consistent with the model from hippocampal cells that phosphorylating APC decreases its function. However, if APC2 were the key substrate, then we would predict that homozygous APC2 mutants, where all APC2 function is lost, should replicate the PP2A phenotype. However, we do not see a synaptic apposition phenotype in recessive mutants for APC2 or in APC1/APC2 double mutants (data not shown). Instead, the enhancement of the PP2A phenotype by the loss of APC2 suggests that APC2 promotes PP2A function, possibly in its role as a scaffolding molecule. Wnt signaling is candidate pathway for mediating these synaptic phenotypes because *wnt* signaling is required for normal *Drosophila* NMJ development and because GSK-3β and PP2A regulate the phosphorylation state of β-catenin in canonical wnt signaling (Packard et al., 2002). Inhibition of PP2A would be predicted to lead to hyperphosphorylation and destruction of β-catenin, thereby blocking *wnt* signaling. However, it is unlikely that the PP2A synaptic phenotype is due to loss of canonical wnt signaling. First, we find that expression of a constitutively active β-catenin (Loureiro et al., 2001) does not suppress the PP2A synaptic phenotype but instead has a slight tendency to enhance the cytoskeletal defect (supplemental Fig. 3, available at www.jneurosci.org as supplemental material). Second, APC functions as part of the destruction complex that leads to degradation of β-catenin and block of *wnt* signaling, however APC mutants enhance rather than suppress the PP2A phenotype. These results are inconsistent with the model that the phenotype is due to decreased canonical *wnt* signaling through β-catenin. However, our data are consistent with a role for β-catenin-independent *wnt* signaling (Ataman et al., 2008; Miech et al., 2008). A third candidate substrate is Futsch, since it can be phosphorylated by GSK-3β (Gögel et al., 2006) and the effect of reduction of PP2A activity on Futsch structure is suppressed by reduction in GSK-3β levels. Continued genetic analysis may lead to the identification of the relevant substrate(s) that are antagonistically regulated by PP2A and GSK-3β to control synaptic development.

There are interesting parallels between the function of PP2A and GSK-3β in the developing *Drosophila* neuromuscular system and in the pathogenesis of neurodegenerative diseases such as Alzheimer's. In *Drosophila*, PP2A antagonizes GSK-3β function to stabilize the synaptic cytoskeleton and promote synapse formation. In models of Alzheimer's disease, PP2A and GSK-3β also act antagonistically, for example in regulating the phosphorylation state of tau (Sontag et al., 1999; Bhat et al., 2004). In addition, disruptions to the axonal cytoskeleton and synapse loss are early events in Alzheimer's pathogenesis. Characterizing the function of PP2A/GSK-3β in regulating cytoskeletal and synaptic integrity during development may provide insights into their role in regulating cytoskeletal and synaptic integrity during disease.

References

Ahmed Y, Hayashi S, Levine A, Wieschaus E (1998) Regulation of armadillo by a *Drosophila* APC inhibits neuronal apoptosis during retinal development. Cell 93:1171–1182.

Ataman B, Ashley J, Gorczyca M, Ramachandran P, Fouquet W, Sigrist SJ, Budnik V (2008) Rapid activity-dependent modifications in synaptic structure and function require bidirectional Wnt signaling. Neuron 57:705–718.

Barth AI, Caro-Gonzalez HY, Nelson WJ (2008) Role of adenomatous polyposis coli (APC) and microtubules in directional cell migration and neuronal polarization. Semin Cell Dev Biol 19:245–251.

Bhat RV, Budd Haeberlein SL, Avila J (2004) Glycogen synthase kinase 3: a drug target for CNS therapies. J Neurochem 89:1313–1317.

Bourouis M (2002) Targeted increase in shaggy activity levels blocks wingless signaling. Genesis 34:99–102.

Broadie K, Bate M (1993) Innervation directs receptor synthesis and localization in *Drosophila* embryo synaptogenesis [see comments]. Nature 361:350–353.

Collins CA, DiAntonio A (2007) Synaptic development: insights from *Drosophila*. Curr Opin Neurobiol 17:35–42.

Daniels RW, Collins CA, Gelfand MV, Dant J, Brooks ES, Krantz DE, DiAntonio A (2004) Increased expression of the *Drosophila* vesicular glutamate transporter leads to excess glutamate release and a compensatory decrease in quantal content. J Neurosci 24:10466–10474.

Eaton BA, Fetter RD, Davis GW (2002) Dynactin is necessary for synapse stabilization. Neuron 34:729–741.

Franco B, Bogdanik L, Bobinnec Y, Debec A, Bockaert J, Parmentier ML, Grau Y (2004) Shaggy, the homolog of glycogen synthase kinase 3, controls neuromuscular junction growth in *Drosophila*. J Neurosci 24:6573–6577.

Füger P, Behrends LB, Mertel S, Sigrist SJ, Rasse TM (2007) Live imaging of synapse development and measuring protein dynamics using two-color fluorescence recovery after photo-bleaching at *Drosophila* synapses. Nat Protoc 2:3285–3298.

Gögel S, Wakefield S, Tear G, Klämbt C, Gordon-Weeks PR (2006) The *Drosophila* microtubule associated protein Futsch is phosphorylated by Shaggy/Zeste-white 3 at an homologous GSK3beta phosphorylation site in MAP1B. Mol Cell Neurosci 33:188–199.

Hamada F, Bienz M (2002) A *Drosophila* APC tumour suppressor homologue functions in cellular adhesion. Nat Cell Biol 4:208–213.

Hannus M, Feiguin F, Heisenberg CP, Eaton S (2002) Planar cell polarization requires Widerborst, a B' regulatory subunit of protein phosphatase 2A. Development 129:3493–3503.

Hurd DD, Saxton WM (1996) Kinesin mutations cause motor neuron disease phenotypes by disrupting fast axonal transport in *Drosophila*. Genetics 144:1075–1085.

Ikeda S, Kishida M, Matsuura Y, Usui H, Kikuchi A (2000) GSK-3beta-dependent phosphorylation of adenomatous polyposis coli gene product

can be modulated by beta-catenin and protein phosphatase 2A complexed with Axin. Oncogene 19:537–545.

Jan LY, Jan YN (1982) Antibodies to horseradish peroxidase as specific neuronal markers in *Drosophila* and in grasshopper embryos. Proc Natl Acad Sci U S A 79:2700–2704.

Janssens V, Goris J (2001) Protein phosphatase 2A: a highly regulated family of serine/threonine phosphatases implicated in cell growth and signalling. Biochem J 353:417–439.

Kittel RJ, Wichmann C, Rasse TM, Fouquet W, Schmidt M, Schmid A, Wagh DA, Pawlu C, Kellner RR, Willig KI, Hell SW, Buchner E, Heckmann M, Sigrist SJ (2006) Bruchpilot promotes active zone assembly, Ca^{2+} channel clustering, and vesicle release. Science 312:1051–1054.

Loureiro JJ, Akong K, Cayirlioglu P, Baltus AE, DiAntonio A, Peifer M (2001) Activated armadillo/beta-catenin does not play a general role in cell migration and process extension in *drosophila*. Dev Biol 235:33–44.

Marrus SB, DiAntonio A (2004) Preferential localization of glutamate receptors opposite sites of high presynaptic release. Curr Biol 14:924–931.

Marrus SB, Portman SL, Allen MJ, Moffat KG, DiAntonio A (2004) Differential localization of glutamate receptor subunits at the *Drosophila* neuromuscular junction. J Neurosci 24:1406–1415.

McCartney BM, Dierick HA, Kirkpatrick C, Moline MM, Baas A, Peifer M, Bejsovec A (1999) *Drosophila* APC2 is a cytoskeletally-associated protein that regulates wingless signaling in the embryonic epidermis. J Cell Biol 146:1303–1318.

Miech C, Pauer HU, He X, Schwarz TL (2008) Presynaptic local signaling by a canonical wingless pathway regulates development of the *Drosophila* neuromuscular junction. J Neurosci 28:10875–10884.

Osterwalder T, Yoon KS, White BH, Keshishian H (2001) A conditional tissue-specific transgene expression system using inducible GAL4. Proc Natl Acad Sci U S A 98:12596–12601.

Packard M, Koo ES, Gorczyca M, Sharpe J, Cumberledge S, Budnik V (2002) The *Drosophila* Wnt, wingless, provides an essential signal for pre- and postsynaptic differentiation. Cell 111:319–330.

Rasse TM, Fouquet W, Schmid A, Kittel RJ, Mertel S, Sigrist CB, Schmidt M, Guzman A, Merino C, Qin G, Quentin C, Madeo FF, Heckmann M, Sigrist SJ (2005) Glutamate receptor dynamics organizing synapse formation in vivo. Nat Neurosci 8:898–905.

Sathyanarayanan S, Zheng X, Xiao R, Sehgal A (2004) Posttranslational regulation of *Drosophila* PERIOD protein by protein phosphatase 2A. Cell 116:603–615.

Schmid A, Hallermann S, Kittel RJ, Khorramshahi O, Frölich AM, Quentin C, Rasse TM, Mertel S, Heckmann M, Sigrist SJ (2008) Activity-dependent site-specific changes of glutamate receptor composition in vivo. Nat Neurosci 11:659–666.

Snaith HA, Armstrong CG, Guo Y, Kaiser K, Cohen PT (1996) Deficiency of protein phosphatase 2A uncouples the nuclear and centrosome cycles and prevents attachment of microtubules to the kinetochore in *Drosophila* microtubule star (mts) embryos. J Cell Sci 109:3001–3012.

Sontag E, Nunbhakdi-Craig V, Lee G, Brandt R, Kamibayashi C, Kuret J, White CL 3rd, Mumby MC, Bloom GS (1999) Molecular interactions among protein phosphatase 2A, tau, and microtubules. Implications for the regulation of tau phosphorylation and the development of tauopathies. J Biol Chem 274:25490–25498.

Stewart BA, Atwood HL, Renger JJ, Wang J, Wu CF (1994) Improved stability of *Drosophila* larval neuromuscular preparations in haemolymph-like physiological solutions. J Comp Physiol A 175:179–191.

Viquez NM, Li CR, Wairkar YP, DiAntonio A (2006) The B' protein phosphatase 2A regulatory subunit well-rounded regulates synaptic growth and cytoskeletal stability at the *Drosophila* neuromuscular junction. J Neurosci 26:9293–9303.

Wagh DA, Rasse TM, Asan E, Hofbauer A, Schwenkert I, Dürrbeck H, Buchner S, Dabauvalle MC, Schmidt M, Qin G, Wichmann C, Kittel R, Sigrist SJ, Buchner E (2006) Bruchpilot, a protein with homology to ELKS/CAST, is required for structural integrity and function of synaptic active zones in *Drosophila*. Neuron 49:833–844.

Wairkar YP, Toda H, Mochizuki H, Furukubo-Tokunaga K, Tomoda T, Diantonio A (2009) Unc-51 controls active zone density and protein composition by downregulating ERK signaling. J Neurosci 29:517–528.

Wu C, Wairkar YP, Collins CA, DiAntonio A (2005) Highwire function at the *Drosophila* neuromuscular junction: spatial, structural, and temporal requirements. J Neurosci 25:9557–9566.

Yao KM, White K (1994) Neural specificity of elav expression: defining a *Drosophila* promoter for directing expression to the nervous system. J Neurochem 63:41–51.

Zhai RG, Bellen HJ (2004) The architecture of the active zone in the presynaptic nerve terminal. Physiology 19:262–270.

Zhou FQ, Zhou J, Dedhar S, Wu YH, Snider WD (2004) NGF-induced axon growth is mediated by localized inactivation of GSK-3beta and functions of the microtubule plus end binding protein APC. Neuron 42:897–912.

Zito K, Parnas D, Fetter RD, Isacoff EY, Goodman CS (1999) Watching a synapse grow: noninvasive confocal imaging of synaptic growth in *Drosophila*. Neuron 22:719–729.